Nanoscale Advances

ROYAL SOCIETY OF CHEMISTRY

PAPER

View Article Online
View Journal | View Issue

Cite this: *Nanoscale Adv.*, 2025, **7**, 6049

Green-synthesized silver nanoparticles from incensole acetate modulate *TPX2* expression in DMBA-induced breast cancer

Iffat Nayila, *[a] Muhammad Sarwar, [b] Saima Hameed, [c] Aasma Iqbal[d] and Sumaira Sharif*[b]

As natural chemicals may have fewer side effects than conventional medicines, their usage in cancer treatment is becoming more popular. Nanoformulations have been the focus of recent developments to increase the anticancer potential of phytocompounds or pure isolated components. To evaluate the anticancer potential of silver nitrate nanoparticles (AgNPs), essential oil (EO) from *Catharanthus roseus* was extracted, a terpene compound was isolated and incensole acetate (IA)-mediated silver nanoparticles (IA-AgNPs) were synthesized. The anticancer potential of biosynthesized IA-AgNPs was assessed using a rat mammary tumor model induced by 9,10-dimethylbenz[*a*]anthracene (DMBA). Scanning electron microscopy (SEM), ultraviolet (UV) and visible spectroscopy, size determination, and dynamic light scattering were used to characterize the synthesized nanoparticles (NPs). To ascertain the bioactive potential of the prepared IA-AgNPs, tests for cytotoxicity, antioxidant activity, stress marker analysis, and histopathology were performed. The study's findings showed that among DMBA-induced rats, IA-AgNPs markedly improved some oxidative stress enzyme levels, and upregulated *TPX2* gene expression. IA-AgNPs demonstrated effective cytotoxicity against MDA-MB-231 cancer cell lines. The anticancer potential was observed by improved levels of antioxidant enzymes. Significant improvements in cancer-induced tissues were found by histopathological investigation, validating the IA-AgNPs' therapeutic effectiveness. In conclusion, the results indicate that *TPX2* gene expression in the DMBA-induced breast cancer (BC) model is altered by biosynthesized silver nitrate NPs. The combined findings highlight IA-AgNPs' promise as a cutting-edge, targeted nanotherapeutic strategy with improved efficacy in treating cancer parameters compared to traditional therapies.

Received 11th April 2025
Accepted 29th July 2025

DOI: 10.1039/d5na00341e

rsc.li/nanoscale-advances

1. Introduction

Anticancer drugs can be delivered and released using smart NPs to target malignancies accurately. However, the fate of the drug-carrying nanocarriers is still a concern. The lungs, kidneys, liver, and heart can all accumulate conventional NPs, depending on their size, shape, surface charge, and whether or not they have a shell surrounding them. The outcome of this deposition is toxicity, which poses a momentous challenge to the production of smart NPs. Only a few human studies have been conducted, but many *in vitro* and *in vivo* toxicity studies have employed animals.[1] Nanotechnology is one of the cutting-edge strategies that has demonstrated exceptional promise in improving cancer treatment through precise drug delivery and molecular targeting. Because of their strong anticancer effects, which include cytotoxicity against cancer cells, induction of apoptosis, and prevention of tumor development, silver NPs have attracted a lot of attention.[2] Nonselective biodistribution, harm to healthy cells or tissues, and drug resistance of cancer cells are the outcomes of traditional cancer treatments like chemotherapy, radiation therapy, and hormone therapy, which calls for high dosages of the drug in the tumor region with little tumor-targeting specificity.[1] On the other hand, new techniques including gene delivery, controlled drug delivery, intracellular drug targeting, tumor-receptor targeting, and triggered drug release, as well as ongoing advancements in cancer drug discovery, have created a useful new range of cancer treatment modalities.[3] Recent developments in nanomedicine have demonstrated that drug delivery based on nanotechnology has significant promise for the diagnosis and treatment of cancer with fewer harmful consequences.[4] Nanoformulations increase the therapeutic efficacy of medications by facilitating drug targeting and direct absorption into cancer cells.[5] NPs are large enough to encapsulate many small-molecule substances, even though they are smaller than cells. At the same time, NPs' vast

[a]*Department of Pharmacy, The University of Lahore Sargodha Campus, Sargodha, Pakistan. E-mail: iffat.nayila5@gmail.com*
[b]*Institute of Molecular Biology and Biotechnology, The University of Lahore, Lahore, Pakistan. E-mail: sumaira.sharif@imbb.uol.edu.pk*
[c]*Institute for Advanced Study, Shenzhen University, Shenzhen, 518060, PR China*
[d]*Department of Zoology, The University of Lahore, Sargodha Campus, Pakistan*

surface area makes them very capable of being functionalized with ligands, such as peptides, small molecules, DNA or RNA.[6] Site-specific target compounds and active controlled-release drug delivery systems that are nanoscale formulations are a few advantages that nanotechnology provides in the treatment of BC.[7] With excellent treatment results, a selection of chemotherapeutics based on NPs have been developed and used therapeutically to treat BC.[8]

The most common malignancy in women, BC accounts for 15% of all cancer deaths. Although the overall survival rate was improved by novel nanotechnology-based techniques, metastatic BC remains difficult to treat, with an anticipated overall survival rate of 23%.[9] Additionally, BC is a different kind of cancer and has been divided into four major subtypes, basal-like BC, HER2-enriched BC, luminal A, and luminal B. As of right now, the following clinically relevant surrogate subtypes were identified by histological and molecular characteristics such as HER2-enriched, luminal A-like, and luminal B-like $HER2^{+}$.[10] Chemotherapy, HER2 targeted therapy or radiotherapy are typically employed in multidisciplinary approaches to treat BC.[11] Various treatment methods for BC frequently have drawbacks such as resistance, toxicity, and recurrence, making it a significant global health concern. Biosynthesized NPs enhance anticancer medications' stability and solubility, which improves treatment results.[12] By avoiding the resistance mechanisms of cancer cells, nanocarriers can increase the effectiveness of treatment in BC. NPs reduce systemic toxicity and adverse responses by regulating medication release.[13] Real-time monitoring of treatment response is made possible by certain NPs that integrate therapy and diagnostics.[14]

TPX2 has been validated as a molecular indicator of a poor patient prognosis. *TPX2* can activate the phosphoinositide 3-kinase/protein kinase B (PI3K/Akt) pathway in breast, ovarian and colon cancer, which in turn can increase the production of the matrix metalloproteinase (MMP) family. According to recent studies, liver cancer cell invasion can be prevented by down-regulating MMP2 and MMP9 expressions in order to suppress *TPX2* expression. *TPX2*'s role in BC is still unknown, though, and little is known about the precise method by which it regulates tumor growth.[15]

The *TPX2* gene, an oncogene implicated in the development of tumors, has become a promising target for treatment; however, there are currently no efficient inhibitors with negligible adverse effects. A natural terpene substance, incensole acetate, having anticancer qualities has demonstrated potential; nonetheless, its limited therapeutic use is due to its poor solubility and absorption. Drug delivery using nanoformulations may increase its efficacy; however, little is known about this strategy. This work investigates how biosynthesized IA-AgNPs may alter *TPX2* expression and the ensuing impacts on the growth and death of BC cells. This study's main goals were to develop and analyze incensole acetate-mediated silver nitrate NPs to assess their efficacy and to determine how effective incensole acetate-mediated NPs are as *TPX2* inhibitors for the treatment of induced BC. This study also investigated how *TPX2* inhibition affects the survival and propagation of BC cells in a DMBA-induced model to evaluate the IA-AgNPs' anti-tumor effectiveness.

2. Methodology

2.1 Essential oil extraction and terpene isolation

Catharanthus roseus (*C. roseus*) plants were collected during the spring (February to April) season. Dr Iftikhar Ahmad deposited a voucher specimen (181-1-23) at the University of Agriculture Faisalabad's Department of Botany for identification. Before being finely milled into powder form (100 g), the gathered plants (5.2 kg) were allowed to air dry for a few days at a temperature between 25 and 28 °C. The hydro-distillation technique was used to extract EO at 100 °C, and the extracted oil was stored between 4 and 6 °C.[16] Multi-dimensional gas chromatography with a capillary column was then used to perform gas chromatography-mass spectrometry (GC-MS) analysis. With the initial temperature set at 250 °C and progressively raised to 280 °C over the course of three minutes, a 0.2 μL sample of EO was injected into the column at a flow rate of 1 μL min^{-1}.[17] Using silica gel 60 (70–250 mesh, Merck) for successive purification, a pure compound from *C. roseus* EO was separated. Acetone, ethyl acetate, dichloromethane, and methanol made up the mobile phase. Using a JEOL JNM-ECA 500 Spectrometer, carbon and proton spectra were acquired at 125 MHz and 500 MHz, respectively, for a nuclear magnetic resonance (NMR) investigation carried out at 25 °C. Version 5.0.4 of the DELTA software was used to document the NMR data (JEOL). The most likely matches from the NIST library were consulted in order to ascertain the structure of the chemical (**https://www.nist.gov/nist-research-library**).[18]

Through a series of purification procedures, the isolated compound from *C. roseus* EO was extracted using silica gel 60 (70–250 mesh, Merck). Acetone, ethyl acetate, dichloromethane, and methanol were used as the process's mobile phase. In order to achieve the best separation, column fractions were examined using thin-layer chromatography (TLC) plates using a solvent system consisting of distilled water and ethyl acetate (4 : 2, v/v). The separated components' retention factor (R_f) values from various fractions were evaluated and aggregated appropriately. Each fraction underwent additional TLC analysis to verify the component's separation.[19]

2.2 Synthesis of silver nitrate nanoparticles

The traditional biogenic technique described by Niraimathi was employed to create IA-AgNPs. AgNPs were made using a silver nitrate ($AgNO_3$) solution and an isolated terpene compound. To create an $AgNO_3$ solution, 0.15 g of $AgNO_3$ was dissolved in 100 mL of distilled water. Before adding the isolated terpene, the $AgNO_3$ solution was shaken for five minutes at room temperature. The solution's color instantly changed from colorless to yellowish brown upon the addition of terpene. This color shift verified the creation of AgNPs, which were subsequently separated by centrifugation for 40 minutes at 14 000 rpm while keeping the temperature at 40 °C.[20] The NPs were then used for further characterization.

2.3 Characterization of nanoparticles

The nano-formulations' medication content, droplet size, and charge potential were all assessed to analyze the physical characteristics and stability of NPs. UV spectrum, droplet size and SEM parametric analyses were also used to determine the homogeneity of nanoparticle droplets.[21]

Photon correlation spectroscopy was used to determine the size distribution of the nano-formulation using a Delsa Nano C Zeta Sizer (Zeta sizer ZS90, Nano-series, Malvern, UK). In order to achieve this, NPs were put into quartz cuvettes that held two milliliters of the sample after being diluted ten times with double-distilled water. 25 °C was the controlled temperature at which the experiment was carried out. IA-AgNP surface charges were measured using a Beckman Coulter Delsa Nano C particle analyzer. The particle charge affected the nanoemulsion's stability and physical characteristics.[22]

Using a UV-visible spectrophotometer at 600 nm absorbance, the turbidity of the NPs was examined.[23] The nanoparticle's shape and structural properties were investigated through the use of SEM at different magnification settings. The samples were prepared by placing a small drop of the biosynthesized formulation onto a spotless glass surface and letting the solvent naturally evaporate at ambient temperature. To examine the surface characteristics, a high-resolution field emission scanning electron microscope (Nova Nano SEM, Japan) was used. The sample was seen at a $1000 \times g$ magnification for SEM imaging, and the voltage was set at 5.00 kV.[24]

2.4 Antioxidant assay

A popular technique for evaluating a compound's antioxidant capability based on its capacity to scavenge free radicals is the 2,2-diphenyl-1-picrylhydrazyl (DPPH) assay. This process involves mixing various quantities of the test material or a standard antioxidant (such as ascorbic acid) with a 0.1 mM DPPH solution that has been added to methanol.[25] A spectrophotometer is used to measure the absorbance at 517 nm after the reaction mixture has been incubated for 30 minutes at room temperature in the dark. The sample's antioxidant capacity is next ascertained by calculating the percentage of DPPH scavenging activity.

For 150 minutes, a reaction mixture including 10 mM sodium nitroprusside (SNP) in phosphate-buffered saline (PBS, pH 7.4) is incubated at 25 °C with varying concentrations of standard antioxidant (ascorbic acid). Following the incubation period, an equivalent volume of Griess reagent, a combination of sulfanilamide and naphthyl ethylenediamine dihydrochloride in acidic conditions, is added to quantify the amount of nitrite that has been produced.[26] At 540 nm, the absorbance is determined with a UV-vis spectrophotometer. The absorbances of the sample and the control are then compared to determine the nitric oxide (NO) scavenging activity as a percentage. By scavenging nitric oxide radicals, this assay sheds light on the potential of bioactive substances to reduce oxidative stress.

The hydrogen peroxide (H_2O_2) scavenging assay assesses a compound's capacity to neutralize the reactive oxygen species hydrogen peroxide. Different quantities of the test sample are combined with a 40 mM H_2O_2 solution in 50 mM phosphate buffer (pH 7.4). A spectrophotometer is used to measure the absorbance at 230 nm following ten minutes of room temperature incubation.[27] The absorbance of the sample and that of the control are then compared to ascertain the scavenging activity. The antioxidant qualities of synthetic substances, natural extracts, and pharmaceutical formulations are all usefully revealed by these assays.

2.5 Antimicrobial activity

Escherichia coli, *Staphylococcus pneumoniae* and *Staphylococcus aureus* bacterial cultures were acquired from the IMBB department, University of Lahore. 40 milliliters of sterile distilled water were used to dissolve a 270 mg tablet of resazurin to create the resazurin solution. A 96-well plate was used for the aseptic test conditions. 100 μL of the sample, comprising 10 mg mL^{-1}, was put onto the plate's first well. After that, the tested sample was diluted and 50 μL of nutritional broth was added to each of the other wells. Each well was then filled with 10 μL of bacterial suspension and 10 μL of resazurin solution. The plates were covered with cling film and incubated for 18 to 24 hours at 37 °C to avoid dehydration.[28] At the lowest concentration at which a color shift occurred, the minimum inhibitory concentration (MIC) was noted. For the terpene IA and the IA-AgNPs, respectively, the negative controls were dimethyl sulfoxide (DMSO) solvent and water–ethanol (1 : 1) solution, whereas the positive control was streptomycin (10 μg/500 μL). Additionally, the nutrient broth served as a negative control.

2.6 *In vitro* assay

The cell lines used for *in vitro* assay were acquired from the Institute of Molecular Biology and Biotechnology Department at The University of Lahore, Lahore, Pakistan. The MDA-MB-231 human cancer cell line and the HMEpC control cell line were cultured in RPMI-1640 medium supplemented with 10% fetal bovine serum, 100 μg mL^{-1} streptomycin, 100 μg mL^{-1} penicillin, and 2 mM L-glutamic acid. The cells were maintained under sterile conditions at 37 °C in a humidified incubator with 5% CO_2. To determine the inhibitory concentration (IC50) value (the concentration required to inhibit a biological process by 50%) and assess cell viability, $AgNO_3$, terpene IA, and IA-AgNPs were tested using the 3-(4,5-dimethylthiazol-2-yl)-2,5-diphenyltetrazolium bromide (MTT) assay, which was modified from the method as described.[29] In both healthy HMEpC cells and MDA-MB-231 cancer cells, the effects of terpene IA and IA-AgNPs on cell viability were assessed in relation to the common chemotherapeutic medication cisplatin. Following their seeding in 96-well plates, the cells were cultured for a full day. Samples were then applied to the cells. The cells were then cultured again in an incubator for a full day. Following a 24 hours exposure to the extracts, 100 μL of MTT solution was added, and then incubated. The monolayer cells were gently rinsed twice with PBS. To dissolve the formazan crystals, 100 μL of DMSO was added to each well. An optical density measurement was made of the samples at 590 nm using a BIOBASE

microplate reader (BioTek-ELx800). Additionally, the IC50 of the samples was determined.[30]

2.7 Crystal violet assay

As stated by the assay,[31] the cytotoxic concentration of the pure compound and biosynthesized IA-AgNPs was determined utilizing the crystal violet staining method to assess the viability of MDA-MB-231 and HMEpC cell lines. Once the culture medium from each experimental group was taken out, the 96-well plate was rinsed with PBS. After that, the wells were filled with a solution containing 0.1% crystal violet dye and 2% ethanol, and they were left to set for 15 minutes at room temperature. Following a thorough cleaning, any excess dye was eliminated from the wells to prevent the cells from separating. After adding 200 μL of 1% SDS to each well to dissolve any remaining dye, the absorbance at 540 nm was measured using a microplate reader.[32]

2.8 *In vivo* anticancer parameters

To induce BC with DMBA, rats were divided into six groups (6 rats per group) and given a freshly made intraperitoneal dose of DMBA (30 mg kg^{-1}) after being randomly assigned to control and experimental groups.[33]

After DMBA was administered, rats were palpated once a week to track the growth of tumors. Following tumor induction and DMBA exposure for 6–8 weeks, the rats were split up into six treatment groups: group 1 acted as the untreated control; group 2 only received the IA-mediated silver NPs (50 mg kg^{-1}); group 3 received DMBA (30 mg kg^{-1}) without any further treatment. Group 4 received DMBA and was treated with IA (20 mg kg^{-1}) dissolved in normal saline after the tumor formed. Group 5 received DMBA and IA-AgNPs (50 mg kg^{-1}) dissolved in normal saline for six weeks, and group 6 comprised DMBA-induced rats that were given cisplatin (5.0 mg kg^{-1}) dissolved in normal saline and administered intraperitoneally.[34] All treatments were administered on alternate days over a six-week period to minimize drug-induced toxicity in the rats.

Weekly tumor growth observations are then made of the animals, and the size and volume of the tumors are regularly calculated. When the treatment period came to an end, the rats in each group were slaughtered. All animals were fasted for 12 hours before having their hearts punctured to get blood. After 20 minutes of coagulation at 4 °C, the blood was centrifuged for 15 minutes at 4000 rpm to extract the serum. The mammary glands were also dissected and stored for histological examination in 5% formalin.

2.9 Tumor weight and tumor growth rate

For four to six weeks after DMBA induction, changes in tumor growth rate were tracked in each experimental group before starting therapy with the terpene and biosynthesized IA-NPs. Tumor size and tumor weight were routinely measured. Tumor growth rate and volume were measured with a Vernier caliper. Tumor volume was computed using length and breadth measures for rats with palpable tumors. By dividing the ultimate tumor size in the treated group by the original tumor volume, the tumor growth ratio (V/V_0) was calculated.[35]

Tumors were palpable four to six weeks later. Weekly tumor development was tracked, and weight and volume changes before and after therapy started were routinely computed. A digital scale and a Vernier caliper were used to measure the tumor's length and volume using the equation

$$\text{Volume} = (\text{width}^2) \times \text{length}/ \quad (2)$$

2.10 Toxicity studies

In accordance with institutional ethical requirements, the acute oral toxicity of the terpene compound and IA-AgNPs is investigated. Rats' liver, kidney, and other bodily organs may be toxically affected by terpene IA, and by IA-AgNPs. For acute toxicity evaluations, such as the complete blood count (CBC), liver function test (LFT), and renal function test (RFT), blood samples were taken from each experimental group. The Cyanomethemoglobin technique was used to measure hemoglobin (Hb). Following established procedures, the red blood cells (RBC), white blood cells (WBC), platelets, and monocytes were measured using a hematological auto-analyzer (Abacus 380).[36] Reitman and Frankel's approach was used to quantify serum alanine aminotransferase (ALT) and serum aspartate aminotransferase (AST) for liver function analysis. An auto-analyzer (Cobas C111 Chemistry Analyzer) was used to measure creatinine and urea levels in order to evaluate kidney function and look into any *in vivo* toxicity effects.[37]

2.11 Oxidative marker analysis

Standardized biochemical assays were used to assess oxidative stress markers, such as glutathione (GSH), malondialdehyde (MDA), nitric oxide (NO), and glutathione peroxidase (GPx). The Griess reagent test was used to measure the NO levels. An equivalent volume of Griess reagent (1% sulfanilamide in 5% phosphoric acid and 0.1% *N*-(1-naphthyl)ethylenediamine dihydrochloride) was combined with tissue homogenate samples. A microplate reader was used to measure the absorbance at 540 nm after the reaction mixture had been incubated for 10 minutes at room temperature. Utilizing a sodium nitrite standard curve, NO values were ascertained.[38]

To measure MDA levels, a measure of lipid peroxidation, the thiobarbituric acid reactive substances (TBARS) assay was used. This procedure involved mixing tissue or serum samples with the thiobarbituric acid (TBA) reagent and heating them in an acidic atmosphere for 30 minutes at 95 °C. A spectrophotometer was used to measure the resulting complex at 532 nm. A 1,1,3,3-tetraethoxypropane standard curve was used to determine the MDA levels.[39]

The Ellman's reagent (5,5′-dithiobis-(2-nitrobenzoic acid), DTNB) test was used to measure the amount of GSH. DTNB was added to tissue homogenate samples, and the absorbance of the resulting yellow complex was measured at 412 nm. A reduced glutathione standard curve was used to calculate the GSH concentration.[40]

Table 1 Primers used for *TPX2* gene expression[a]

Target genes	Sequencing	PCR product size	Primer temperature, °C
TPX2 forward	AACAATCCATTCCGTCAA	332 bp	51.62
TPX2 reverse	TGCAGGTGGCATACAAGG		57.26
GAPDH forward	ACCTGACCTGCCGTCTAGAA	247bp	57.20
GAPDH reverse	TCCACCACCCTGTTGCTGTA		57.15

[a] *GAPDH* = reference housekeeping gene, PCR = polymerase chain reaction, bp = base pair.

To assess GPx activity, a linked enzyme reaction was used. NADPH in phosphate buffer, glutathione reductase, and GSH were all present in the reaction mixture. At 340 nm, the drop in NADPH absorbance was measured when H_2O_2 was added to start the enzyme process.[41]

2.12 *TPX2* expression analysis

The expression of the *TPX2* gene was examined using the real-time polymerase chain reaction (RT-PCR) method. Tissue samples were used to extract total RNA for RT-PCR using a commercial RNA isolation kit and the manufacturer's instructions.[42] Components of the RNA/primer mix are presented in ESI Table S1. RNA's purity and concentration were measured with a Nanodrop spectrophotometer at 260/280 nm. From 1 μg of total RNA, complementary DNA (cDNA) was produced using a reverse transcription kit. SYBR Green Master Mix, cDNA, *TPX2* gene-specific primers, and nuclease-free water were utilized for RT-PCR in a 10 μL reaction volume. The amplification was performed in a thermal cycler under the following conditions: initial denaturation at 95 °C for 5 minutes, 40 cycles of denaturation at 95 °C for 15 seconds, annealing at an ideal temperature (55–60 °C) for 30 seconds, and extension at 72 °C for 20 seconds. The $2^{-\Delta\Delta C}$T technique was utilized to examine the relative expression levels of *TPX2*, while *GAPDH* served as an internal reference gene.[43] Following each experiment, expression analysis was measured, and the data were normalized using the *GAPDH* expression in these samples. ESI Table S2 displays the temperatures and thermal cycler cycles that were recorded, and the lists of primers used, their order, and product size are noted in Table 1.

2.13 Polymerase chain reaction

From extracted DNA samples, target gene sequences were amplified using the PCR. Following the manufacturer's instructions, genomic DNA was extracted from tissue samples using a commercial DNA extraction kit. The extracted DNA's content and purity were evaluated at 260/280 nm using a Nanodrop spectrophotometer. 50 ng of template DNA, 200 μM of each dNTP, 0.5 μM of forward and reverse primers, 1 unit of Taq DNA polymerase, 10× PCR buffer with $MgCl_2$, and nuclease-free water to adjust the final volume were all used in the 25 μL reaction mixture used for PCR amplification. The first 30 to 35 cycles of denaturation occurred at 95 °C for 30 seconds, followed by annealing at an ideal temperature (50 to 65 °C) for 30 seconds, extension at 72 °C for 1 minute, and a final extension step at 72 °C for 10 minutes. Using 1.5% agarose gel electrophoresis, ethidium bromide staining, and UV trans-illuminator visualization, the PCR products were examined. As a molecular weight marker, a 100 bp DNA ladder was employed to verify the anticipated amplicon size. All tests were carried out in triplicate, and negative controls which lacked template DNA were included to rule out contamination and guarantee the precision and repeatability of the data.

2.14 Histopathology

Rats used in the experiment had their breast tissues carefully removed for histological examination. Following a 24 to 48 hour cleaning with PBS, they were promptly preserved in 10% neutral buffered formalin. Tissues were fixed, dehydrated using a graded ethanol sequence, cleaned in xylene, and embedded in paraffin wax to create tissue blocks. Thin slices (4–5 μm) were then cut with a rotary microtome and put on glass slides. The slices were rehydrated using progressively lower ethanol concentrations, deparaffinized with xylene, and stained with hematoxylin and eosin (H&E) to assess morphological changes, cellular architecture, and potential tissue damage.[44] Under a light microscope, stained sections were viewed at various magnifications to evaluate structural changes, tumor growth, fibrosis, and other histological features. Using a digital imaging device, photomicrographs were taken for comparison. The degree of histopathological alteration was rated using standard criteria to gauge tissue damage and treatment results.[45]

2.15 Statistical analysis

Both the means and the standard error of the mean (SEM) are shown. The groups treated with isolated terpene and IA-AgNPs, the DMBA-induced group, and the experimental control group were all statistically compared. Prism software version 9.5 (GraphPad Software, San Diego, CA, USA) was utilized for statistical analysis, which involved a *post hoc* Dunnett test. The following criteria were used to determine statistical significance: $p < 0.05$, $p < 0.001$, and $p < 0.0001$.

3. Results

3.1 GC-MS analysis

After the EO of *C. roseus* was extracted using the hydro-distillation process, its chemical makeup was examined using GC-MS. In order to effectively separate the EO's volatile components and guarantee that heat-sensitive chemicals degraded as little

as possible, hydro-distillation was used. Comprehensive chromatographic profiles from the GC-MS analysis are shown in ESI Fig. S1 and Table S3, which show the different chemical components found using this method.[17] This was confirmed by the results of the GC-MS analysis. *C. roseus* contains a large number of different bioactive compounds. The primary components discovered were terpenes, flavonoids, terpenoids, alkanes, and aldehydes, and these substances contribute to the EO's distinct potential biological effects. These findings are consistent with previous studies that detailed the complex composition of *C. roseus* EO emphasizing its possible applications in various fields.

3.2 Terpene compound identification and characterization

TLC and silica gel column chromatography were used to isolate the terpene IA from *C. roseus* EO. R_f values of isolated terpene obtained from EO are presented in ESI Table S4. The chemical was then refined by column chromatography, which separated the EO components according to their polarity. Initially, TLC was utilized to track the separation process and detect the presence of IA. In line with previously published values in the literature, the isolated IA's retention index (RI) was found to be 2173.[17] Acetone, methanol, and ethyl acetate were combined in a 5.1 : 3.9 : 1.0 ratio to perform TLC analysis of the separated fraction. A stretching vibration at 1643 cm^{-1} was visible in the infrared (IR) spectrum, suggesting the existence of a carbonyl functional group. Furthermore, the IR results verified that the molecule included sp^2 hybridized carbon. Unsaturated bonds were indicated by signals at 1436 cm^{-1}, whereas a C–O stretching band was represented by a peak at 1376 cm^{-1}. ESI Fig. S2 shows the results of the analysis of the compound's chemical structure for the proton nuclear magnetic resonance (^{1}H-NMR) spectrum, and ESI Fig. S3 shows the results for the carbon-13 nuclear magnetic resonance (^{13}C-NMR) spectrum. The molecular weight of isolated terpene (IA) was calculated to be 334 g mol^{-1}. A molecular ion peak at 348 amu was found by mass spectrometry analysis, which is consistent with observations that have been previously published.[17]

3.3 Optimization and nanoparticle characterization

IA-AgNPs were synthesized by adjusting the concentrations of isolated terpene (1.5 mM) and silver nitrate (0.15 g), at the reaction temperature (35 to 60 °C) for 40–50 minutes. The pH of the reaction medium is adjusted at 6.10–7.12. These conditions yielded 90% IA-mediated NPs with an average size of 116 nm, demonstrating stability and uniform dispersion as also verified by SEM, zeta potential and UV-visible studies. These parameters typically influence synthesis and the representative values are also mentioned in ESI Table S5.

The synthesized IA-AgNPs were stored at 25 ± 4 °C (room temperature), and preliminary testing indicated that IA-AgNPs were stable. The pH, viscosity and zeta potential of IA-AgNPs were analyzed (Table 2). The synthesized NPs seemed to be polydisperse in size, with an average, characteristic peak seen at 116.0 nm (ESI Fig. S4). IA-AgNPs were visible, and the PDI of IA-AgNPs was found to be 0.420 with an average range of 0.3 to 0.420. ESI Fig. S5 also displays the zeta potential data of the IA-AgNPs, which showed a single significant peak and a shift to −18.3 (mV). The color of NPs is pale yellow at the time of preparation and a slight color variation was also observed in IA-AgNPs after 24 and 48 hours of placement (ESI Fig. S6).

There is a wide absorption peak with a wavelength of 535 nm shown in the UV-visible spectra of IA-AgNPs with absorbance at 2.27 (ESI Fig. S7). It was shown that the nanoparticle's wavelength was within the required range, indicating the production of small sized NPs.[3] The form and size distribution of IA-loaded silver NPs (IA-AgNPs) were examined using SEM (Fig. 1). SEM imaging revealed a complex structure, offering important insights into the NPs' morphological properties. SEM analysis gives a representation of NPs ranging in diameter from 120 nm to 163 nm, and it was observed that IA-AgNPs had a uniform and random size distribution. According to SEM analysis, the uniform and spherical assembly of IA-AgNPs indicates that the final structure of the NPs is greatly influenced by the interaction

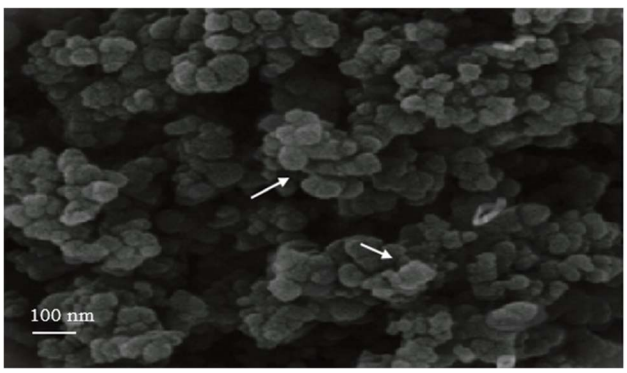

Fig. 1 SEM representation of IA-AgNPs.

Table 2 Physical parameters and characterization of IA-AgNPs[a]

	Parameters				
Duration	pH ± SD	Viscosity (mPa s) ± SD	Zeta size (nm)	Zeta Potential (mV)	Appearance
24 hours	6.14 ± 0.02	2.23 ± 0.12	116.0	−18.3	Brownish yellow
48 hours	6.11 ± 0.01	2.23 ± 0.12	116.0	−18.1	Dark brown
72 hours	6.11 ± 0.02	2.33 ± 0.12	116.0	−18.0	Dark brown

[a] mPa s = millipascal seconds (units of viscosity).

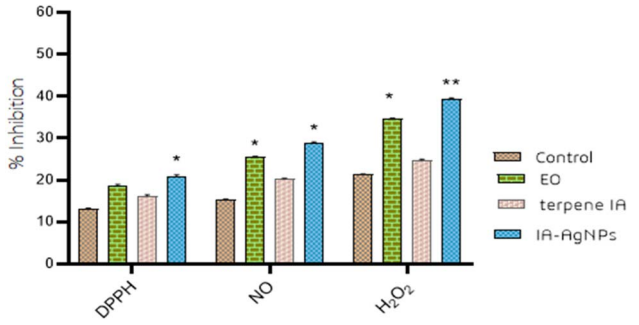

Fig. 2 DPPH and free radical assay. Significant values indicating * (p < 0.05), ** (p < 0.001), and *** (p < 0.0001).

Table 3 Anti-bacterial activity (estimated MIC values)[a]

No.	Bacterial species MIC(μg mL^{-1})
1	*E.coli* + terpene IA 240 ± 1 : 32
2	*E.coli* + IA-AgNPs 320 ± 1 : 41**
3	*S. pneumoniae* + terpene IA 260 ± 2 : 04
4	*S. pneumoniae* + IA-AgNPs 340 ± 1 : 44**
5	*S. aureus* + terpene IA 240 ± 2 : 22
6	*S. aureus* + IA-AgNPs 320 ± 1 : 41**

[a] MIC values, where **p < 0.001 as compared to the standard streptomycin. MIC = minimum inhibitory concentration.

between IA and silver nitrate ions during their production. Interconnected particles may increase surface area and reactivity, which may affect the stability and functional characteristics of the NPs. Generally speaking, the NPs have a uniform size range, contingent on synthesis parameters including temperature and concentration of synthetic agents. Effective stabilization, frequently accomplished by capping agents that inhibit excessive aggregation, is shown by the homogeneity of shape and dispersion of NPs.

3.4 Dpph antioxidant activity

Fig. 2 displays the outcomes of terpene IA, and IA-AgNPs' inhibition of different radicals. In every scavenging test, IA-AgNPs exhibited the highest antioxidant activity when compared to the control, with a p-value of 0.001. Results showed that silver nitrate NPs of IA have the greatest H_2O_2 and NO scavenging activity compared to their DPPH scavenging activity. These outcomes were contrasted with the standard reagent ascorbic acid. According to the findings, *C. roseus* EO's antioxidant properties may be attributed to the presence of various secondary metabolites. The silver NPs mediated by IA showed notable antioxidant activity in comparison to ascorbic acid, the common antioxidant used as a control. The results indicate that the synthesized NPs may be capable of effectively scavenging DPPH and preventing oxidative damage (p < 0.05). The NO and H_2O_2 radical scavenging activity of IA-AgNPs was high. In the presence of biosynthesized IA-AgNPs, the assay medium demonstrated effective scavenging of H_2O_2 (p < 0.001) and NO (p < 0.05). These results suggest that NPs can effectively scavenge NO, H_2O_2, and DPPH radicals, potentially providing protection against oxidative damage.

3.5 Antimicrobial activity

The antibacterial properties of terpene IA and the synthesized IA-AgNPs were analyzed by calculating estimated MIC values and by growth inhibition data. Bacterial species *E. coli*, *S. pneumoniae* and *S. aureus* were tested for the possible antibacterial activity of IA-AgNPs. Table 3 provides the estimated MIC values recorded in the presence of the IA-mediated silver nitrate NPs and isolated terpene compound. With IA-AgNPs, the estimated MIC values against *E. coli*, *S. pneumoniae*, and *S. aureus* were between 240 and 340 μg mL^{-1} (Table 3). The estimated MIC values in the presence of the synthesized NPs were comparable to those of the isolated IA-compound.

The bacterial growth response to the terpene compound and IA-loaded silver nitrate nanoparticles (IA-AgNPs) of concentrations 1–500 μg mL^{-1} is shown in Table 4. A visual depiction of the microtiter test plates is provided in ESI Fig. S8, emphasizing the antibacterial growth (+) and no growth (−) representation of terpene IA and IA-AgNPs. According to the findings, silver NPs showed strong antibacterial action, successfully preventing the growth of *S. pneumoniae*, *E. coli*, and *S. aureus*. Interestingly, the

Table 4 Anti-bacterial assay of growth (+) and no growth (−)

No	Bacterial species growth of bacteria									
		Terpene IA								
	Concentration (μg mL^{-1})	500	250	100	50	25	10	1	Negative control	Streptomycin (10 μg/500 μL)
1	*E. coli*	−	−	−	−	−	+	+	+	−
2	*S. pneumoniae*	−	−	−	+	+	+	+	+	−
3	*S. aureus*	−	−	−	−	−	+	+	+	−
	IA-AgNPs									
1	*E. coli*	−	−	−	−	−	−	−	+	−
2	*S. pneumoniae*	−	−	−	−	−	−	−	+	−
3	*S. aureus*	−	−	−	−	−	−	−	+	−

best inhibitory activity against these bacterial species was shown at the highest concentration (500 μg mL^{-1}).

3.6 Cytotoxicity analysis

The length and concentration of application determine the anti-proliferative effect of biosynthesized silver nitrate NPs of IA on MDA-MB231 cancer cell lines and HMEpC healthy cells. Using varying concentrations of tested substances, the cytotoxicity of IA and IA-AgNPs was examined. The viability of cells treated with IA-AgNPs was significantly higher than that of cells treated with silver nitrate solution, with a *p*-value of less than 0.001 (Fig. 3A). The anti-proliferative effect of IA-AgNPs on MDA-MB-231 cancer cell lines and HMEpC healthy epithelial cells depends on the application's time and concentration. IA-AgNPs produced significant results; however, $AgNO_3$ solution and terpene IA also showed cytotoxic and harmful effects on malignant cell lines. In the MDA-MB-231 cell lines, IA-AgNPs showed cytotoxicity at the highest doses. The results showed that IA exhibited substantial cytotoxicity where $p < 0.05$, while IA-AgNPs had significantly high cytotoxicity at 1.5 μg mL^{-1} concentration.

HMEpC cells had an appreciable effect on cell viability after 48 hours at IA-AgNPs with significant viability $p < 0.05$. In cancer cell lines, as shown in Fig. 3B, the IC_{50} significantly dropped after 48 hours as opposed to 24 hours. When using MDA-MB-231 cancer cell lines, the IC_{50} concentration for IA-AgNPs at 1 μg mL^{-1} was 37.48, and for IA-AgNPs at 1.5 μg mL^{-1} it was 26.21. There was a substantial difference in the cytotoxic effects between the control group and IA-AgNPs, as evidenced by the statistically substantial difference in statistically calculated IC_{50} values ($p < 0.001$). When compared to the 24 hours mark, the IC_{50} values for IA-AgNPs were significantly lower after 48 hours ($p < 0.0001$), indicating a gradual increase in cytotoxicity. Greater inhibitory power is indicated by a significantly lower IC_{50} value, indicating that IA-AgNPs efficiently decrease cell viability even at lower concentrations. After 48 hours, there was a significant difference ($p < 0.001$) in the cytotoxicity of IA-AgNPs against MDA-MB-231 cells compared to the control. Cell death dramatically increased when the concentration of NPs reached 1.5 μg mL^{-1}.

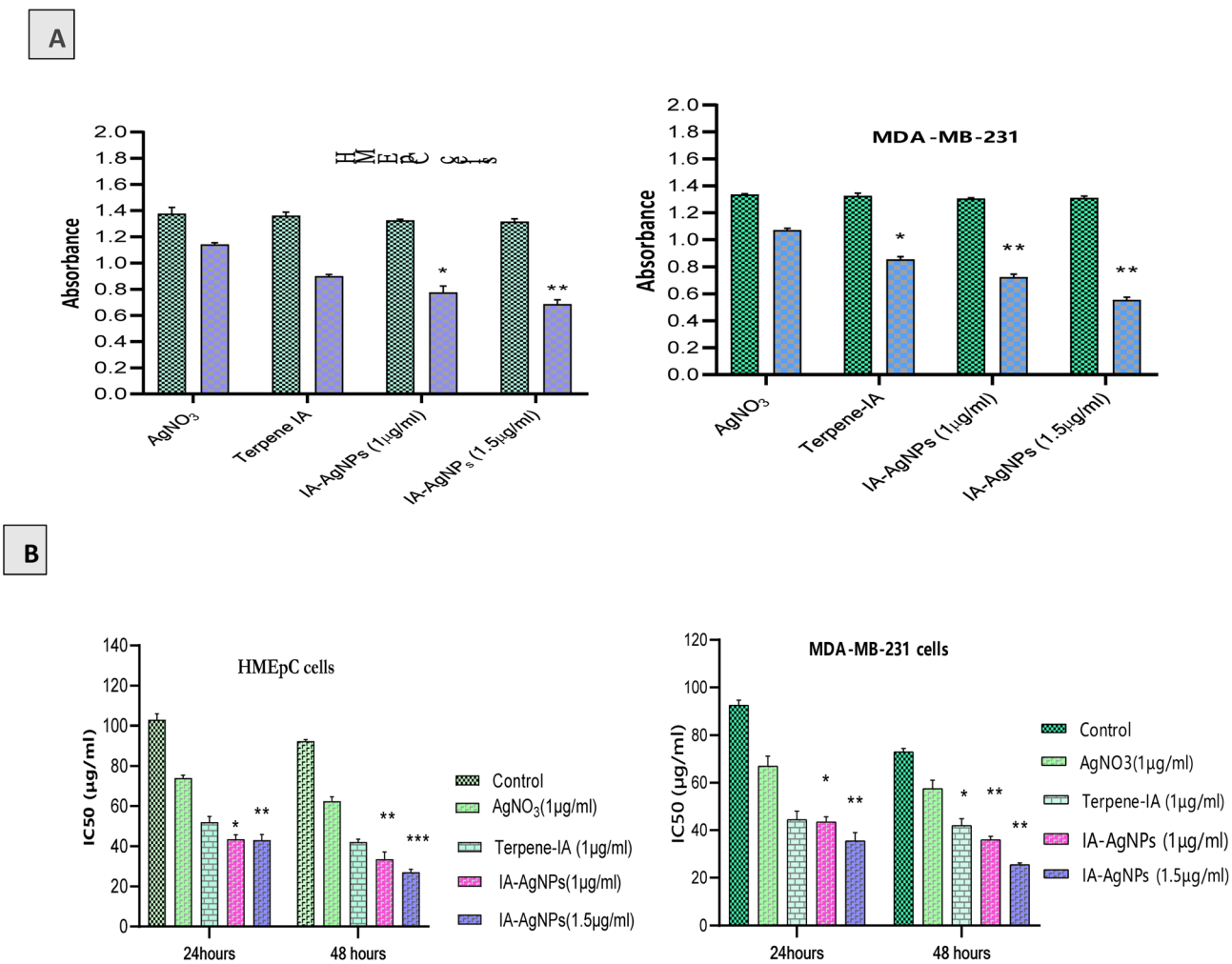

Fig. 3 (A) MTT-based cytotoxicity assay and (B) IC50 analysis. Mean ± standard deviation values are shown, with * ($p < 0.05$), ** ($p < 0.001$), and *** ($p < 0.0001$) indicating significance compared to the control and DMBA-induced groups.

3.7 Crystal violet assay

The vitality of HMEpC and MDA-MB-231 cancer cells after treatment with varying dosages of IA-AgNPs was evaluated using the crystal violet assay. In comparison to the untreated control group, the results showed a considerable decrease in the quantity of viable cancer cells. The vitality of HMEpC healthy epithelial cells responded differently to IA-AgNP treatment. In comparison to the control group, HMEpC cells exhibited a statistically significant decrease in viability ($p < 0.05$) when treated with IA alone. Furthermore, a more noticeable effect was observed when IA-AgNPs were exposed at a concentration of 1.5 μg mL^{-1}, as cell viability was significantly lower ($p < 0.001$) compared to untreated healthy cells. In particular, compared to untreated MDA-MB-231 cells, IA-AgNPs at a concentration of 1 μg mL^{-1} showed a statistically significant increase in absorption ($p < 0.05$) and a considerable loss in cell viability (Fig. 4). On the other hand, IA-AgNPs showed significantly more cytotoxic effects on cancer cells at a higher dose of 1.5 μg mL^{-1}, exhibiting highly significant cytotoxicity ($p < 0.001$). According to these results, cancer cells are more severely impacted by IA-AgNPs' selective cytotoxicity than healthy epithelial cells.

3.8 Tumor weight and growth

Following six weeks of treatment, the effect of IA-AgNPs on tumor progression was assessed, and Fig. 5 shows the tumor weight and total tumor burden. Animals given solely the carcinogen (DMBA) in the DMBA-induced cancer paradigm showed an average breast tumor weight that accounted for 64.60% of their total body weight. On the other hand, animals in the control group and IA-mediated NP group did not acquire any tumors, indicating that DMBA treatment did not cause tumor formation. These control groups served as a starting point for evaluating how terpene IA and silver nitrate NPs affected the development of tumors. Groups treated with IA-AgNPs showed a significantly lower tumor incidence than the DMBA-only control group ($p < 0.05$). IA-AgNP therapy also resulted in a significant reduction in tumor weight, lowering the tumor burden to an average of 46.10% ($p < 0.05$), suggesting that it may have anticancer efficacy. In accordance with the well-established chemotherapeutic effects of cisplatin, rats that received therapy showed an even higher reduction in tumor incidence ($p < 0.001$) when compared to the untreated DMBA-induced group. IA-AgNPs and cisplatin demonstrated the strongest inhibitory effects on tumor development and weight loss among the studied therapies. According to these results, IA-AgNPs have the potential to be a potent anticancer drug that provides a targeted treatment approach with notable tumor-suppressive capabilities. The fundamental mechanisms of IA-AgNPs in tumor inhibition and their possible synergistic effects with traditional chemotherapy require more research.

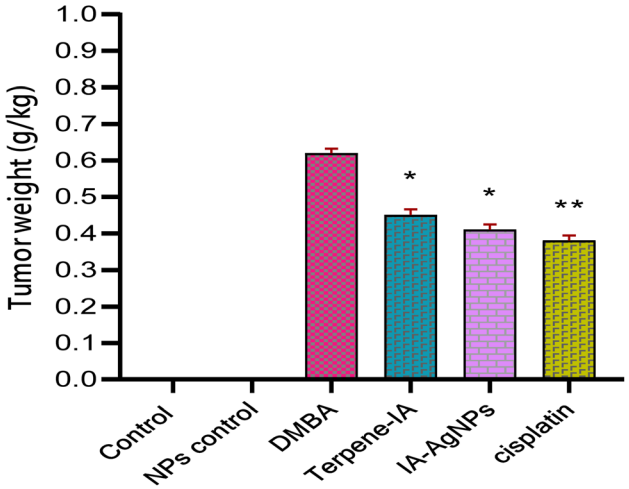

Fig. 5 Tumor weight in experimental groups. Mean ± standard deviation values are shown, with * ($p < 0.05$), ** ($p < 0.001$), and *** ($p < 0.0001$) indicating significance compared to the control and DMBA-induced groups.

Nanoparticles' effects on tumor volume show the effect of IA-mediated silver nitrate NPs on tumor characteristics as in Table 5. Experimental rats in the control group had a lower tumor incidence than DMBA-induced rats ($p < 0.001$). The IA-NP-

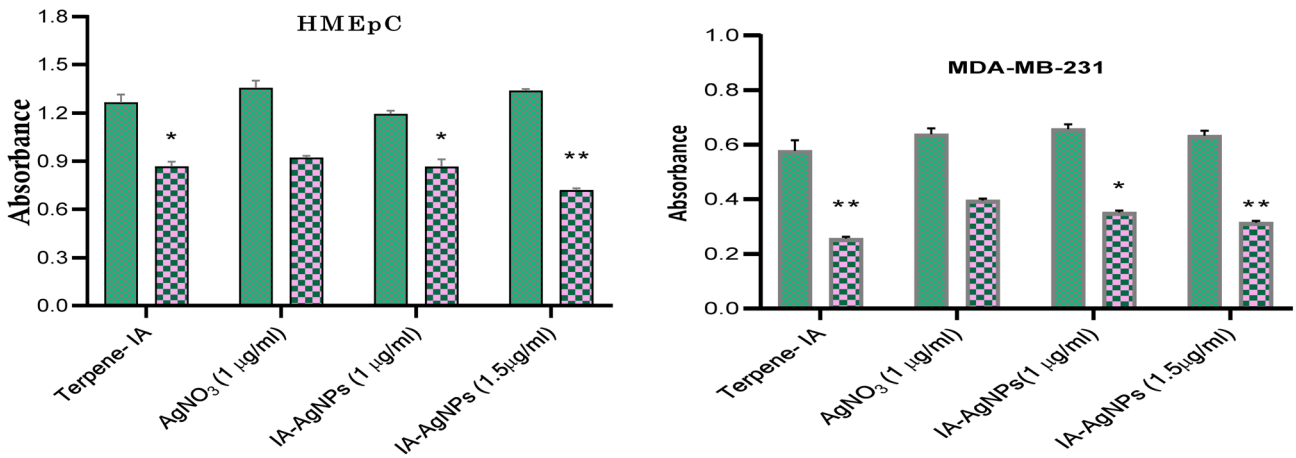

Fig. 4 Crystal violet assay. Mean ± standard deviation values are shown, with * ($p < 0.05$), ** ($p < 0.001$), and *** ($p < 0.0001$) indicating significance compared to the control and DMBA-induced groups.

Table 5 Effect of synthesized IA-AgNPs on tumor parameters

Parameters	Control	NPs control	DMBA	DMBA + terpene-IA	DMBA + IA-AgNPs	DMBA + Cisplatin
Tumor volume mm^3 (pre-treatment)	0	0	8.422	8.322	8.413	8.532
Tumor volume mm^3 (post- treatment)	0	0	9.366	6.744	6.733	6.011
Tumor ratio	0	0	0.899	0.810	0.800	0.704

Table 6 Effect of IA-AgNPs on hematological parameters[a]

Parameters	Control	NPs control	DMBA	DMBA + terpene-IA	DMBA + IA-AgNPs	DMBA + cisplatin
RBCs ($\times 10^6$ μL)	7.4 ± 0.05	7.42 ± 0.08	11.13 ± 0.13	9.82 ± 0.11*	9.32 ± 0.54	9.41 ± 0.33
Platelets ($\times 10^3$ μL)	931.00 ± 13.01	1133 ± 14.8	1543 ± 12.8	1422 ± 10.9*	1287 ± 12.9*	1534 ± 13.98
WBCs ($\times 10^3$ μL)	11.10 ± 0.25	11.21 ± 0.41	16.04 ± 0.22**	11.76 ± 0.43*	11.41 ± 0.11*	14.76 ± 0.73
Hb (g dL^{-1})	13.07 ± 0.31	15.5 ± 0.21	11.5 ± 0.22*	14.3 ± 0.13	13.2 ± 0.13	16.1 ± 0.71
Monocytes (%)	2.11 ± 0.22	3.14 ± 0.12	4.5 ± 0.43	4.3 ± 0.54	4.2 ± 0.13	3.46 ± 0.94*
Neutrophils (%)	24.50 ± 1.12	32.1 ± 2.11	31 ± 2.42	31 ± 2.31	34 ± 2.34	26 ± 2.21*

[a] Values are expressed as mean ± SEM ($n = 6$), with significance levels indicated by symbols: * ($p < 0.05$), ** ($p < 0.001$), and *** ($p < 0.0001$).

treated group and cisplatin group treated showed a significant decrease in tumor size, with a p-value less than 0.05.

3.9 Hematology and toxicity parameters

Rats treated with IA, IA-AgNPs, and cisplatin had their hematological parameters evaluated after DMBA-induced cancer developed in order to determine the effects of these treatments (Table 6). Hemoglobin levels in the IA-AgNP-treated group differed from those in the DMBA-induced control group but this is statistically non-significant ($p > 0.05$). In particular, IA-AgNPs markedly decreased platelet levels ($p < 0.001$) and the total WBC count ($p < 0.001$), indicating possible impacts on the immune system and coagulation mechanisms. In contrast to the DMBA-induced group, rats treated with IA-AgNPs had notable improvements in several hematological parameters, such as Hb levels and platelet count. Animals treated with IA-AgNPs resulted in a significant recovery in platelet and WBC counts, demonstrating the potential of IA-AgNPs to lessen the hematological abnormalities brought on by DMBA-induced malignancy. These results highlight the advantages of IA-AgNPs in bringing cancer-treated rats' blood cell parameters back to normal, offering insight into their potential as a treatment. In view of the safety and toxicity profile, these findings collectively underscore the necessity of a comprehensive understanding of the biosynthesized nanoparticles' impact on hematological parameters and urge further investigation into the mechanisms and potential consequences.

3.9.1 Liver function test. When LFT results were compared across treatment groups and the control group in the toxicity trial, minor variations in liver markers were found, and overall, statistically significant alterations were found. Table 7 demonstrates that there were significant variations within the DMBA-induced group. The possible influence of tumor formation and subsequent treatment on liver enzyme activity was demonstrated by the considerably higher ALT levels in the IA-AgNPs group (72 ± 0.40) as compared to the control group (52 ± 0.13; $p < 0.05$). This suggests a slight impact on liver function, which may be connected to the metabolic requirements of the tumor and the therapy itself. AST levels also exhibited a moderate rise in the IA-AgNPs group (142 ± 0.35 compared to the DMBA group) and a considerable increase in the DMBA group (161 ± 0.23 compared to the control group). Although these alterations are significant enough ($p < 0.05$) to suggest DMBA toxicity, they may be related to hepatic stress brought on by tumor induction. A slight impact on bilirubin metabolism was also showed by the non-significant rise in bilirubin levels in the IA-AgNPs treatment group (0.55 ± 0.12) when compared to the control group (0.5 ± 0.30). In contrast to the DMBA-induced control group, the IA-AgNPs group showed a significant increase (0.77 ± 0.31), indicating some influence on bilirubin processing. Although the IA-AgNPs treatment caused modest changes in liver function markers, the overall influence on liver health was low, as evidenced by the mild changes in albumin levels that were statistically significant. These results imply that IA-AgNPs

Table 7 Liver function tests[a]

Parameter	Control	NPs control	DMBA	DMBA + terpene-IA	DMBA + IA-AgNPs	DMBA + cisplatin
ALT (μ L^{-1})	52 ± 0.13	54 ± 0.13	77 ± 0.40*	83 ± 0.40*	72 ± 0.40*	66 ± 0.40*
AST (μ L^{-1})	121 ± 0.11	126 ± 0.34	161 ± 0.23**	167 ± 0.31 *	142 ± 0.35*	134 ± 0.30**
Bilirubin (mg dL^{-1})	0.5 ± 0.22	0.43 ± 0.22	0.77 ± 0.31	0.41 ± 0.31	0.55 ± 0.12	0.46 ± 0.24**
Albumins (mg dL^{-1})	0.12 ± 0.01	0.23 ± 0.13	0.4 ± 0.21*	0.32 ± 0.12	0.36 ± 0.23*	0.35 ± 0.13*

[a] Values expressed as mean ± SEM ($n = 6$). Symbols indicated significant levels as * (0.05), ** (0.001) and *** (0.0001).

Table 8 Renal function tests[a]

Parameter	Control	NPs control	DMBA	DMBA + terpene-IA	DMBA + IA-AgNPs	DMBA + Cisplatin
Blood urea (mmol L^{-1})	6.5 ± 1.6	6.4 ± 0.8	9.3 ± 0.6*	8.5 ± 0.9	6.5 ± 0.2*	6.2 ± 0.4*
Serum creatinine (mmol L^{-1})	67.2 ± 2.2	64.6 ± 3.2	84.0 ± 4.2**	71.0 ± 4.1	61.0 ± 3.1*	74.0 ± 3.2

[a] Values expressed as mean ± SEM ($n = 6$). Symbols indicated significant levels as * (0.05), ** (0.001) and *** (0.0001).

therapy does not result in severe hepatic toxicity, despite minor changes in liver function tests. The noted alterations, however, underscore the significance of more research into the long-term impacts of IA-AgNPs on liver function and the dosage's safety. To completely assess the NPs' impact on hepatic functions and guarantee their safety for therapeutic usage, more research is required.

3.9.2 Renal function test. When compared to the control and DMBA-administered groups, the RFTs in the toxicity study showed statistically significant differences between the treatment groups. Blood urea levels were significantly lower in the IA-AgNPs treatment group (6.2 ± 0.2) than in the DMBA group (9.3 ± 0.6) and similarly lower in the cisplatin-treated group (6.4 ± 0.4) after both treatments were administered (Table 8). These results imply that IA-AgNPs may have an impact on urea metabolism, resulting in decreased blood urea levels. Furthermore, the group treated with IA-AgNPs had significantly lower serum creatinine levels (61.0 ± 3.1) than the DMBA-induced control group (84 ± 4.2). IA-AgNPs may have a minor impact on kidney function and enhance creatinine clearance, according to this evidence. IA-AgNPs administration led to a significant reduction in both urea and creatinine levels ($p < 0.05$) when compared to the DMBA group overall, indicating that IA-AgNPs may have a positive impact on renal function under tumor-induced stress. Further investigation into the safety and renal benefits of IA-AgNPs in therapeutic settings is necessary in light of these findings.

3.10 Stress marker analysis

Rats in a tumor-associated stress state brought on by DMBA had their antioxidant markers measured. Comparing the IA-AgNPs

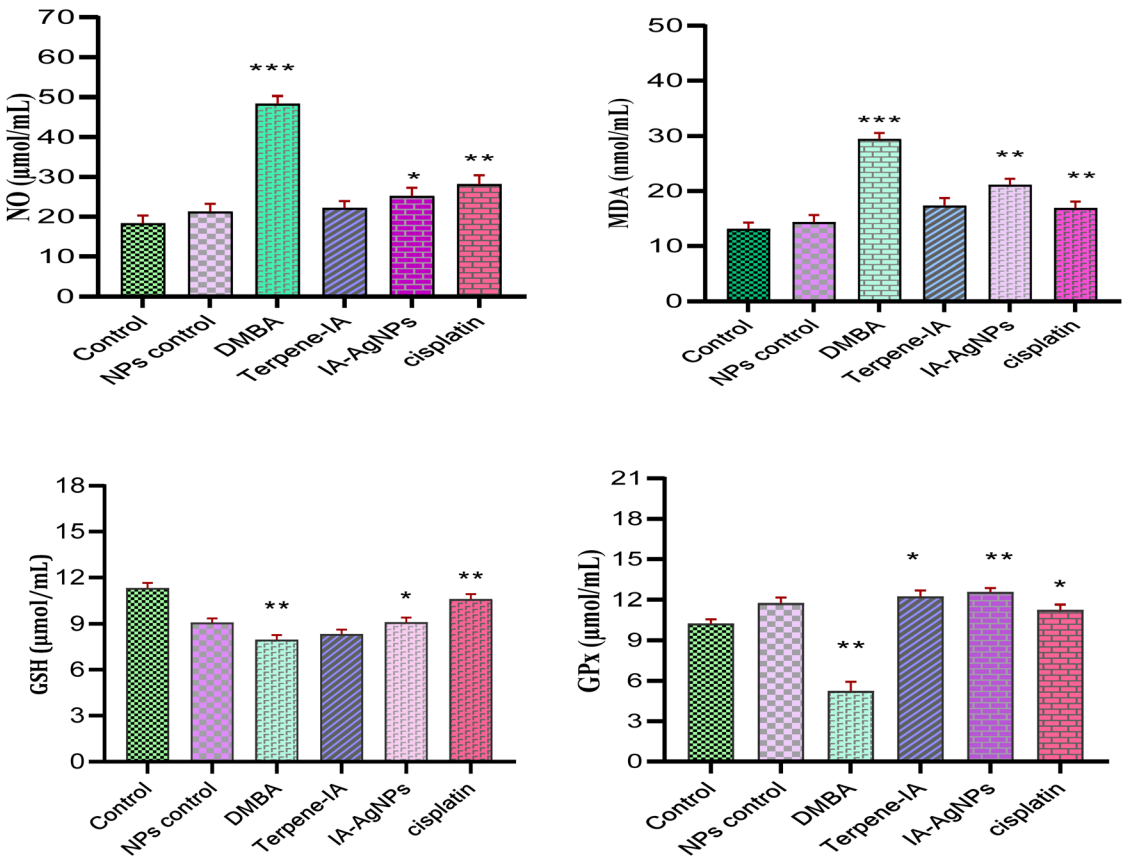

Fig. 6 Stress markers in IA-AgNPs treated rats. Mean ± standard deviation values are shown, with * ($p < 0.05$), ** ($p < 0.001$), and *** ($p < 0.0001$) indicating significance compared to the control and DMBA-induced groups.

and cisplatin treatment groups to the normal control and DMBA-induced control groups, the results revealed substantial differences in a number of stress markers (Fig. 6). When compared to the DMBA-induced group, the IA-AgNPs and cisplatin-treated groups showed a substantial decrease in NO levels. In particular, NO levels dropped considerably in the group treated with IA-AgNPs ($p < 0.05$) and even more in the group treated with cisplatin ($p < 0.001$). The cisplatin-treated group exhibited a statistically significant increase ($p < 0.001$) in the restoration of normal NO levels. In comparison to the normal control group, the DMBA-induced group had significantly higher levels of MDA activity, a sign of oxidative stress ($p < 0.0001$). On the other hand, MDA levels were significantly decreased by both IA-AgNPs and cisplatin therapy; IA-AgNPs' improvement was similar to that of the cisplatin-treated group ($p < 0.0001$). Similar to the effects of cisplatin therapy, these results imply that IA-AgNPs administration effectively reduces oxidative stress in animals with cancer. The IA-AgNPs group had considerably higher GSH levels than the DMBA-induced group ($p < 0.05$). Although GSH levels were likewise raised by IA therapy, there was no statistically significant difference ($p > 0.05$). GSH levels in the cisplatin-treated group increased the greatest, reaching 10.60 U g^{-1} ($p < 0.0001$), demonstrating the powerful anti-oxidative effects of the drug. Lastly, the tumor-associated oxidative stress was reflected in the considerably lower GPx levels in the DMBA-induced rats ($p < 0.001$). GPx activity increased significantly with both IA-AgNPs and cisplatin therapy, where $p < 0.001$ for IA-AgNPs, $p < 0.05$ for IA, and IA administration significantly outperformed the DMBA-induced group ($p < 0.05$). Furthermore, DMBA + cisplatin-treated rats showed a considerable increase in GPx levels, which is in line with the enhancements reported in the control and DMBA-induced-groups.

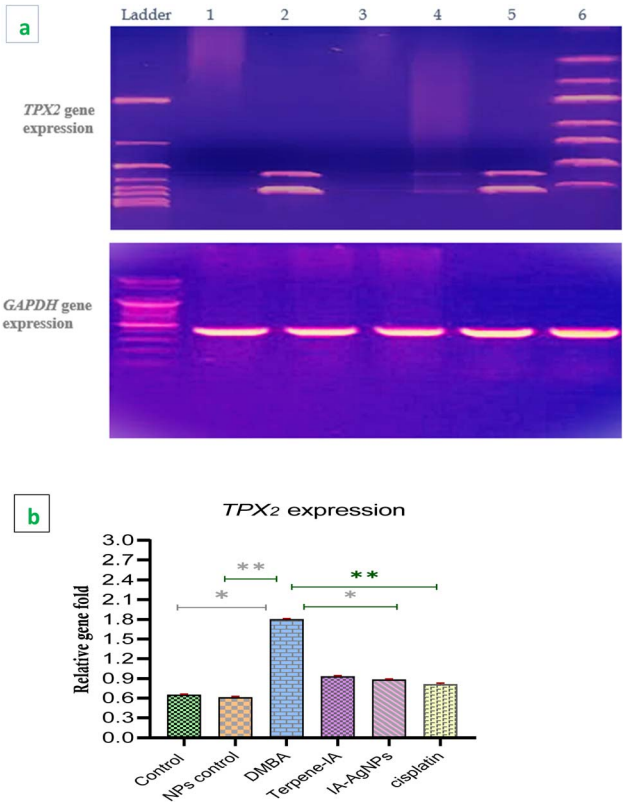

Fig. 7 (a); *TPX2* expression in control and IA-AgNPs treated groups. (b) Graphical illustration of fold change in *TPX2* expression. Mean ± standard deviation values with * ($p < 0.05$), ** ($p < 0.001$), and *** ($p < 0.0001$) indicating significance compared to the vehicle and DMBA-induced groups.

3.11 Gene expression analysis of *TPX2*

Compared to the DMBA-induced group, rats treated with IA, IA-AgNPs, and the chemotherapeutic agent cisplatin showed a substantial decrease in *TPX2* gene expression. Both IA ($p < 0.001$) and cisplatin ($p < 0.001$) significantly reduced *TPX2* expression, and IA-AgNPs likewise significantly decreased ($p < 0.05$). *GAPDH* was the housekeeping gene; its expression was relatively stable, so it was used for gene expression analysis (Fig. 7a). The density ratio of each *TPX2* band with *GAPDH* was computed in the present study and a graphical representation of *TPX2* expression levels is shown in Fig. 7b to assess the impact of biosynthesized IA-AgNPs on DMBA-induced cancer animals. Additionally, *TPX2* expression levels in rats receiving IA and IA-AgNPs were considerably lower ($p < 0.05$) when compared directly to the DMBA-induced group, indicating a downregulation effect on this gene. The DMBA control group and the nanoparticle-treated control group showed differences in *TPX2* expression, but these differences were not statistically significant.

3.12 Histopathology of mammary tissues

The glandular ductal network that makes up the mammary gland is bordered by a protective layer of epithelial cells, which exhibit hyperplasia when damaged and produce inflammation in cancer-induced animals. Rats in the normal control group showed mammary tissue with normal structure and clearly defined architecture.[42] According to the histology data, the normal architecture of mammary tissue indicates that DMBA treatment damages healthy breast tissues shown in Fig. 8A. Rats in the DMBA-induced cancer group displayed epidermal ulceration and neutrophil inflammation (Fig. 8B). All of the cancer-induced rats in this group had ductal carcinoma with localized proliferation, and glandular cell multiplication. The groups treated with IA-AgNPs and drug cisplatin are depicted in Fig. 8C and D. A lymph node demonstrating the effacement of the lymph node architecture was seen in the group that received IA-AgNPs at a dose of 50 mg kg^{-1}. The broad infiltration of lymphoid cells obliterated the architecture. Additionally, erythrophagocytosis was seen in several locations in these areas. It was observed that some fibrous connective tissues also surround the cancerous cells of mammary tissues and are also permissible in the nuclei of small mononucleated cells. The DMBA-carcinogenesis group's acini with intralobular septa regenerated after receiving silver nitrate NP treatment. The ability to reconstruct the stroma and the normal structure of the acini were indicators of this progress (Fig. 8C).

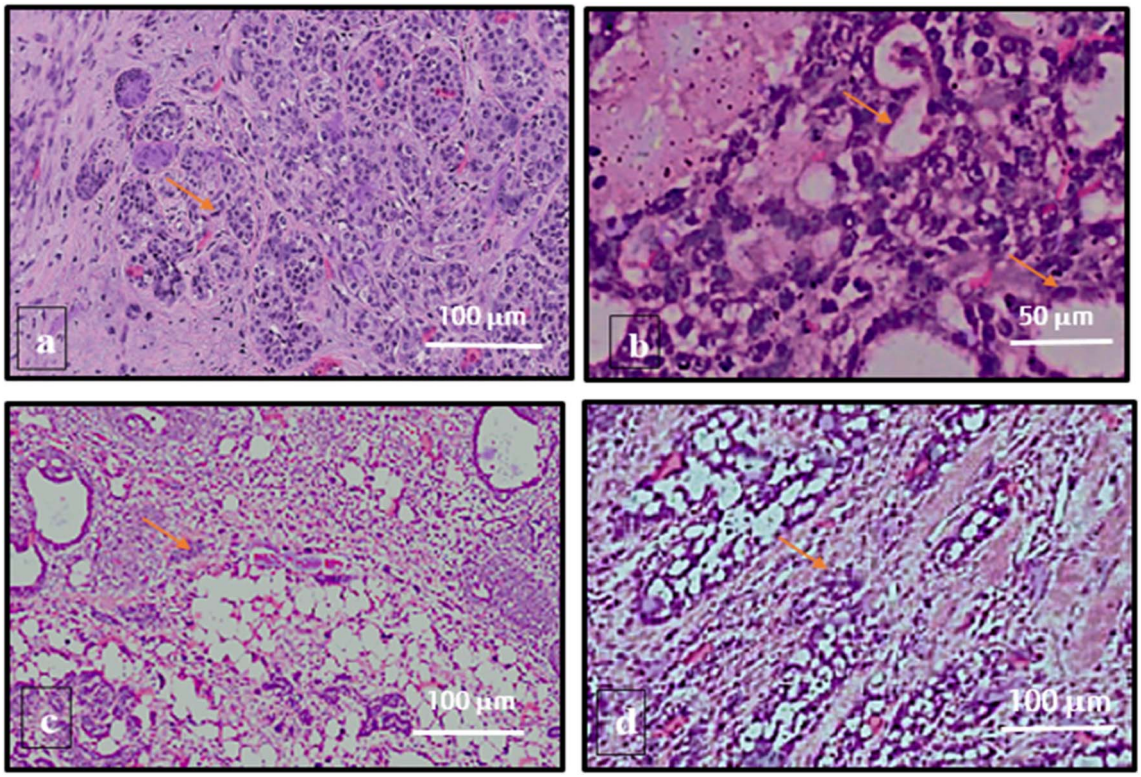

Fig. 8 Histological imaging of mammary glands of experimental animals (A: control; B: DMBA-induced; C: IA-AgNPs treated; and D: drug cisplatin-treated). (A) A layer of epithelial cells indicated by arrows typically covers the breast tissues in the control group, and the ductal lumen is empty. There were no dilated acini with ducts seen in the mammary tissues. (B) Dysplasia and cancer cell infiltration into the mammary stroma are signs of neoplastic cell development on the mammary alveoli. The duct's surface displayed hyperplasia in this group. (C) Numerous dilated acini and ductal epithelial cells that were somewhat larger than normal cells were found, along with improvement in hyperplasia of the tumor cells. (D) The cisplatin-treated group had less dilatation and a normal structure, and there were indications of improvement and acini regeneration.

4. Discussion

When deciding which treatment approach is best, it is crucial to consider the subtypes, stage and grade of BC, age, and medical conditions of the patients. The primary goals of treatment for metastatic and non-metastatic BC are tumor eradication, recurrence and metastasis prevention.[45] Generally speaking, systemic and local treatment are part of BC's typical therapeutic approach.[11] It was found that *TPX2* downregulation by siRNA can prevent BC cells from proliferating, invading, and migrating by preventing MMP2 and MMP9 expression. However, more research is still needed to determine the precise molecular process and the relationship between *TPX2* and prognosis.[46] Research indicates that *TPX2* can stimulate tumor development, growth, and distant metastases in addition to tumor formation, incidence, and progression.[15] Numerous human malignancies, including hepatocellular carcinoma, bladder carcinoma, prostate cancer, and metastatic BC, have been shown to overexpress *TPX2*, a protein necessary for microtubule assembly and mitosis. Tumor development and metastasis are significantly influenced by this overexpression.[47] One study found that, in comparison to normal tissue, *TPX2* was significantly overexpressed in 129 out of 203 (60.8%) colorectal cancer (CRC) metastatic lesions. Additionally, there was a correlation between *TPX2* overexpression and poorer overall and metastasis-free survival, vascular invasion, and metastasis. *TPX2* inhibition reduced the ability of cancer cells to proliferate, become tumorigenic, migrate, and invade both *in vitro* and *in vivo*.[48] A possible therapeutic impact in DMBA-induced cancer models is suggested by the observed downregulation of *TPX2* expression in groups treated with IA and IA-AgNPs. Overexpression of *TPX2* has been connected to a number of cancers, and it is well known to be essential for the growth of tumors.[49] The substantial decrease in *TPX2* expression following treatment with IA and IA-AgNPs is consistent with other research showing the anticancer potential of medications derived from plants and their nanoparticle formulations. The observed reduction in *TPX2* levels is similar to that reported with the common chemotherapeutic drug cisplatin, suggesting that IA-based treatments are effective in modifying oncogenic pathways.

In contrast to chemical or physical approaches, the green synthesis method is a quick mode to produce NPs with significant outcomes like reduced toxicity, biocompatibility, and environmental friendliness.[50] By means of the green synthesis approach, silver nitrate NPs are created using the biocomponents of plants, living cells or isolated compounds of natural herbal plants.[51] Biosynthesized NPs have some other modest advantages, such as high biocompatibility, greater stability, UV absorption capabilities, and antibacterial and

anticancer potential.[52] Using the synthesized IA-AgNPs, the cytotoxic, tumor-related and anti-proliferative effects in DMBA-induced BC were evaluated in our presented study. The anti-proliferative, anti-inflammatory, anti-tumor, and antioxidant properties of EOs which are abundant in terpenes and terpenoids have long been acknowledged.[53] It was essential to investigate the nanoformulation's potential in a cancer model for improved and targeted delivery of nano-based therapies, given the strong characteristics of these pure isolated compounds.[54] The IA-AgNPs' promise as an efficient anticancer drug is demonstrated by the notable decrease in tumor incidence and burden that occurs after treatment. By inducing oxidative stress and activating apoptosis, silver NPs have been shown to have lethal effects on cancer cells.[2] The observed tumor suppression is consistent with research showing that IA can alter important signaling pathways implicated in carcinogenesis and has potent anti-proliferative effects.[55] Additionally, IA-AgNPs' similar effectiveness to that of cisplatin implies that these NPs could be a viable substitute or supplement to traditional chemotherapy, thereby lowering toxicity without sacrificing therapeutic value.[56]

A study indicated that the volume and weight of DMBA-induced tumors were significantly decreased after a nano-curcumin formulation was administered. Additionally, there was also a decrease in Akt phosphorylation, tumor growth factor-β (TGF-β), PI3K, and cancer gene expression.[57] It was determined by the current investigation that by lowering oxidative stress indicators and raising antioxidant enzyme levels in tumor-induced rats, IA-AgNPs showed a strong anti-oxidative impact. These findings imply that IA-AgNPs may be a useful therapeutic agent that can manage oxidative stress linked to the advancement of cancer, on par with or even better than cisplatin. In support of this evidence, it is stated that curcumin, a similar terpene compound and biosynthesized NPs of curcumin have also been shown to exhibit a variety of pharmacological effects in both *in vitro* and *in vivo* tests, including anti-inflammatory, antioxidant, antibacterial and antiviral qualities.[58] Despite having important biological characteristics, curcumin's low solubility, quick systemic elimination, poor bioavailability, and limited targeted specificity severely limit its medicinal use but it was found that the synthetic NPs of curcumin have better therapeutic potential with fewer side effects.[3] As a result, a wide range of intelligent NPs are currently in use or may be used in the future as drug delivery vehicles for cancer treatments. Clinicians are now able to offer novel treatments or incorporate them as additives to therapies that are already working well because of their unique characteristics. This study has shown that IA-mediated silver nitrate NPs hold promise in creating safer and effective cancer treatments to reduce tumor burdens in cancer-induced models. Future research should examine how IA-AgNPs interact molecularly with carcinogenic pathways and evaluate how well they work in combination with currently available chemotherapeutic drugs. However, long-term thinking and the development of innovative cancer treatment strategies such as co-delivery of combinational medications, stimuli-responsive drug release, and targeted drug delivery may be aided by future investigations on these isolated compounds' nano-formulations.

5. Conclusion

The current study demonstrates the noteworthy anticancer potential of IA-AgNPs made using EO from *C. roseus*. In DMBA-induced BC models, the biosynthesized IA-AgNPs efficiently decreased tumor burden, increased antioxidant enzyme activity such as MDA, GSH and GPx, and controlled tumor growth rate and tumor parameters. Additionally, the NPs demonstrated significant cytotoxicity against MDA-MB-231 cancer cell lines. IA-AgNPs effectively inhibited the expression of the *TPX2* gene, which is essential for the progression of cancer cells. IA-AgNPs' therapeutic effectiveness in ameliorating tissue changes brought on by cancer was also validated by a histopathological investigation. These results imply that IA-AgNPs may be effective therapeutic agents for the treatment of BC. The safety and effectiveness of treatment may be impacted by the complete consideration of immunogenicity, long-term consequences, and possible off-target accumulation. Thus, additional research including clinical trials is required to confirm these results and guarantee their translational relevance. To confirm their effectiveness and to determine their potential for clinical use, further molecular and clinical research is also necessary.

Ethical approval

This study was previously approved by the Institution of Molecular Biology and Biotechnology, Bioethical, Biosafety and Biosecurity Committee of Department of Molecular Biology and Biotechnology, University of Lahore with reference number CRiMM/23/Research/32 and is in accordance with research guidelines of IMBB, TUOL.

Author contributions

Conceptualization, writing original draft preparation: Iffat Nayila; resources and data investigation: Sumaira Sharif; data curation, review and editing: Sumaira Sharif, Saima Hameed and Aasma Iqbal; supervision, project administration: Sumaira Sharif, Iffat Nayila and Muhammad Sarwar. All authors have read and agreed to the published version of the manuscript.

Conflicts of interest

The authors declare no conflict of interest.

Data availability

We declare that all the data generated are included in this study.

The SI contains additional experimental data, detailed methodology, extended, raw datasets, and tables supporting the findings of this study. These materials are available online alongside the published article. See DOI: **https://doi.org/10.1039/d5na00341e**.

Abbreviations

C. roseus	*Catharanthus roseus*
EO	Essential oil
GC/MS	Gas chromatography-mass spectrometry
IA-AgNPs	Incensole acetate mediated silver nanoparticles
HER2	Human epidermal growth factor receptor 2
MDA-MB-231	Epithelial, human breast cancer cell line
MTT	Dimethylthiazol diphenyltetrazolium
NPs	Nanoparticles

References

1 L. Sun, H. Liu, Y. Ye, Y. Lei, R. Islam, S. Tan, et al., Smart nanoparticles for cancer therapy, *Signal Transduction Targeted Ther.*, 2023, **8**(1), 1–28.
2 H. I. O. Gomes, C. S. M. Martins and J. A. V. Prior, Silver nanoparticles as carriers of anticancer drugs for efficient target treatment of cancer cells, *Nanomaterials*, 2021, **11**(4), 964.
3 W. Yang, H. Veroniaina, X. Qi, P. Chen, F. Li and P. C. Ke, Soft and condensed nanoparticles and nanoformulations for cancer drug delivery and repurpose, *Adv. Ther.*, 2020, **3**(1), 1900102.
4 T. Jiang, K. M. Gonzalez, L. E. Cordova and J. Lu, Nanotechnology-enabled gene delivery for cancer and other genetic diseases, *Expert Opin. Drug Delivery*, 2023, **20**(4), 523–540.
5 I. Nayila, S. Sharif, M. S. Lodhi, R. Ullah, A. Alotaibi and T. Maqbool, Targeting the *WWP1* gene with incensole acetate nanoemulsion: a novel therapeutic strategy for breast cancer, *S. Afr. J. Bot.*, 2024, **172**, 415–429.
6 N. Rashidi, M. Davidson, V. Apostolopoulos and K. Nurgali, Nanoparticles in cancer diagnosis and treatment: progress, challenges, and opportunities, *J. Drug Delivery Sci. Technol.*, 2024, **95**, 105599.
7 X. Tang, W. S. Loc, C. Dong, G. L. Matters, P. J. Butler, M. Kester, et al., The use of nanoparticulates to treat breast cancer, *Nanomed*, 2017, **12**(19), 2367–2388.
8 V. Jain, H. Kumar, H. V. Anod, P. Chand, N. V. Gupta, S. Dey, et al., A review of nanotechnology-based approaches for breast cancer and triple-negative breast cancer, *J. Controlled Release*, 2020, **326**, 628–647.
9 R. Verma, K. Kumar, S. Bhatt, M. Yadav, M. Kumar, P. Tagde, et al., Untangling breast cancer: trailing towards nanoformulations-based drug development, *Recent Pat. Nanotechnol.*, 2025, **19**(1), 76–98.
10 N. Harbeck, Breast cancer is a systemic disease optimally treated by a multidisciplinary team, *Nat. Rev. Dis. Primer*, 2020, **6**(1), 1–2.
11 F. Yang, Q. He, X. Dai, X. Zhang and D. Song, The potential role of nanomedicine in the treatment of breast cancer to overcome the obstacles of current therapies, *Front. Pharmacol.*, 2023, **14**, 1143102, Available from: **https://www.frontiersin.org/journals/pharmacology/articles/10.3389/fphar.2023.1143102/full**.
12 S. Montazersaheb, A. Eftekhari, A. Shafaroodi, S. Tavakoli, S. Jafari, A. Baran, et al., Green-synthesized silver nanoparticles from peel extract of pumpkin as a potent radiosensitizer against triple-negative breast cancer (TNBC), *Cancer Nanotechnol.*, 2024, **15**(1), 47.
13 S. K. Verma, E. Jha, P. K. Panda, A. Thirumurugan, S. Patro, S. K. S. Parashar, et al., Molecular insights to alkaline based bio-fabrication of silver nanoparticles for inverse cytotoxicity and enhanced antibacterial activity, *Mater. Sci. Eng., C*, 2018, **92**, 807–818.
14 F. Bahman, V. Pittalà, M. Haider and K. Greish, Enhanced anticancer activity of nanoformulation of dasatinib against triple-negative breast cancer, *J. Pers. Med.*, 2021, **11**(6), 559.
15 Y. Yang, D. P. Li, N. Shen, X. C. Yu, J. B. Li, Q. Song, et al., TPX2 promotes migration and invasion of human breast cancer cells, *Asian Pac. J. Trop. Med.*, 2015, **8**(12), 1064–1070.
16 A. Ashmawy, N. Mostafa and O. Eldahshan, GC/MS analysis and molecular profiling of lemon volatile oil against breast cancer, *J. Essent. Oil Bear. Plants*, 2019, **22**(4), 903–916.
17 I. Nayila, S. Sharif, M. Shahzad Lodhi, M. F. Ur Rehman and F. Aman, Synthesis, characterization and anti-breast cancer potential of an incensole acetate nanoemulsion from *Catharanthus roseus* essential oil; *in silico*, *in vitro*, and *in vivo* study, *RSC Adv.*, 2023, **13**(46), 32335–32362.
18 P. An, X. Yang, J. Yu, J. Qi, X. Ren and Q. Kong, α-terpineol and terpene-4-ol, the critical components of tea tree oil, exert antifungal activities *in vitro* and *in vivo* against *Aspergillus niger* in grapes by inducing morphous damage and metabolic changes of fungus, *Food Control*, 2019, **98**, 42–53.
19 Y. L. Ngo and L. S. Chua, Column chromatography for preparing rosmarinic acid rich extract from *Orthosiphon aristatus*, *J. Liq. Chromatogr. Relat. Technol.*, 2019, **42**(17–18), 546–554.
20 K. L. Niraimathi, V. Sudha, R. Lavanya and P. Brindha, Biosynthesis of silver nanoparticles using *Alternanthera sessilis* (Linn.) extract and their antimicrobial, antioxidant activities, *Colloids Surf., B*, 2013, **102**, 288–291.
21 A. V. M. Abadi, E. Karimi, E. Oskoueian, G. R. K. S. Mohammad and N. Shafaei, *Synthesis, Characterization and Cytoxicity Evaluation of Syzygium aromaticum L. Bud (clove) Essential Oil Nanoemulsion*, In Review, 2021, Available from: **https://www.researchsquare.com/article/rs-952488/v1**.
22 S. Bhattacharjee, DLS and zeta potential – What they are and what they are not?, *J. Controlled Release*, 2016, **235**, 337–351.
23 O. Uncu, B. Ozen and F. Tokatli, Use of FTIR and UV-visible spectroscopy in determination of chemical characteristics of olive oils, *Talanta*, 2019, **201**, 65–73.
24 G. Crippa, F. Ye and C. Malinverno, Which is the best method to prepare invertebrate shells for SEM analysis? Testing different techniques on recent and fossil brachiopods, *Boll. Della Soc. Paleontol. Ital.*, 2016, (2), 111–125.

25 A. Karagöz, F. T. Artun, G. Özcan, G. Melikoğlu, S. Anıl, Ş. Kültür, et al., *In vitro* evaluation of antioxidant activity of some plant methanol extracts, *Biotechnol. Biotechnol. Equip.*, 2015, **29**(6), 1184–1189.

26 A. M. T. Gusti, S. Y. Qusti, E. M. Alshammari, E. A. Toraih and M. S. Fawzy, Antioxidants-related superoxide dismutase (SOD), catalase (CAT), glutathione peroxidase (GPX), glutathione-s-transferase (GST), and nitric oxide synthase (NOS) gene variants analysis in an obese population: a preliminary case-control study, *Antioxidants*, 2021, **10**(4), 595.

27 C. D. Fernando and P. Soysa, Optimized enzymatic colorimetric assay for determination of hydrogen peroxide (H_2O_2) scavenging activity of plant extracts, *MethodsX*, 2015, **2**, 283–291.

28 S. Sinha, S. Das, B. Saha, D. Paul and B. Basu, Anti-microbial, anti-oxidant, and anti-breast cancer properties unraveled in yeast carotenoids produced *via* cost-effective fermentation technique utilizing waste hydrolysate, *Front. Microbiol.*, 2023, **13**, 1088477, Available from: **https://www.frontiersin.org/journals/microbiology/articles/10.3389/fmicb.2022.1088477/full**.

29 M. Ravi, M. K. Sneka and A. Joshipura, The culture conditions and outputs from breast cancer cell line *in vitro* experiments, *Exp. Cell Res.*, 2019, **383**(2), 111548.

30 C. Luis, Y. Castaño-Guerrero, R. Soares, G. Sales and R. Fernandes, Avoiding the interference of doxorubicin with MTT measurements on the MCF-7 breast cancer cell line, *Methods Protoc.*, 2019, **2**(2), 29.

31 T. Maqbool, S. J. Awan, S. Malik, F. Hadi, S. Shehzadi and K. Tariq, *In vitro* anti-proliferative, apoptotic and antioxidative activities of medicinal herb kalonji (*Nigella sativa*), *Curr. Pharm. Biotechnol.*, 2019, **20**(15), 1288–1308.

32 V. Vandersickel, J. Slabbert, H. Thierens and A. Vral, Comparison of the colony formation and crystal violet cell proliferation assays to determine cellular radiosensitivity in a repair-deficient MCF10A cell line, *Radiat. Meas.*, 2011, **46**(1), 72–75.

33 A. Alhoshani, M. Alotaibi, H. M. As Sobeai, N. Alharbi, K. Alhazzani, A. Al-Dhfyan, et al., *In vivo* and *in vitro* studies evaluating the chemopreventive effect of metformin on the aryl hydrocarbon receptor-mediated breast carcinogenesis, *Saudi J. Biol. Sci.*, 2021, **28**(12), 7396–7403.

34 M. V. Shirmanova, I. N. Druzhkova, M. M. Lukina, V. V. Dudenkova, N. I. Ignatova, L. B. Snopova, et al., Chemotherapy with cisplatin: insights into intracellular pH and metabolic landscape of cancer cells *in vitro* and *in vivo*, *Sci. Rep.*, 2017, **7**(1), 8911.

35 A. Talkington and R. Durrett, Estimating tumor growth rates *in vivo*, *Bull. Math Biol.*, 2015, **77**(10), 1934–1954.

36 F. Abedi Tameh, H. E. A. Mohamed, L. Aghababaee, M. Akbari, S. Alikhah Asl, M. H. Javadi, et al., *In vitro* cytotoxicity of biosynthesized nanoceria using *Eucalyptus camaldulensis* leaves extract against MCF-7 breast cancer cell line, *Sci. Rep.*, 2024, **14**(1), 17465.

37 Z. Mehboob, S. Sharif, M. S. Lodhi, A. B. Shah, M. Romman and I. Nayila, Phytochemical profiling and anticancer potential of gardenia latifolia extracts against arsenic trioxide induced liver fibrosis in rat model, *Front. Pharmacol.*, 2024, **15**, 1389024, Available from: **https://www.frontiersin.org/journals/pharmacology/articles/10.3389/fphar.2024.1389024/full**.

38 H. Danesh, N. Ziamajidi, S. A. Mesbah-Namin, N. Nafisi and R. Abbasalipourkabir, Association between oxidative stress parameters and hematological indices in breast cancer patients, *Int. J. Breast Cancer*, 2022, **2022**(1), 1459410.

39 A. Burwaiss, M. Ammar, R. Alghazeer, A. Eljamil, D. Alarbie, S. Elghmasi, et al., Tissue levels of oxidative stress markers and antioxidants in colorectal cancer patients, *Main Group Chem.*, 2022, **21**(2), 491–499.

40 E. Jablonska, J. Gromadzinska, B. Peplonska, W. Fendler, E. Reszka, M. B. Krol, et al., Lipid peroxidation and glutathione peroxidase activity relationship in breast cancer depends on functional polymorphism of GPX1, *BMC Cancer*, 2015, **15**(1), 657.

41 K. A. Amin, B. M. Mohamed, M. A. M. El-wakil and S. O. Ibrahem, Impact of breast cancer and combination chemotherapy on oxidative stress, hepatic and cardiac markers, *J. Breast Cancer*, 2012, **15**(3), 306–312.

42 L. Khorsandi and M. Farasat, Zinc oxide nanoparticles enhance expression of maspin in human breast cancer cells, *Environ. Sci. Pollut. Res.*, 2020, **27**(30), 38300–38310.

43 N. Masood, F. A. Malik and M. A. Kayani, Unusual intronic variant in GSTP1 in head and neck cancer in Pakistan, *Asian Pac. J. Cancer Prev. APJCP*, 2012, **13**(4), 1683–1686.

44 A. H. Aalami, M. Mesgari and A. Sahebkar, Synthesis and characterization of green zinc oxide nanoparticles with antiproliferative effects through apoptosis induction and MicroRNA modulation in breast cancer cells, *Bioinorg. Chem. Appl.*, 2020, **2020**, e8817110.

45 D. P. Henry, J. Ranjan, R. K. Murugan, A. Sivanantham and M. Alagumuthu, Exploration of anti-breast cancer effects of *Terminalia chebula* extract on DMBA-induced mammary carcinoma in sprague dawley rats, *Future J. Pharm. Sci.*, 2020, **6**(1), 108.

46 J. Cheng, The TPX2 gene is a promising diagnostic and therapeutic target for cervical cancer, *Oncol. Rep.*, 2012, **27**, 1353–1359, Available from: **http://www.spandidos-publications.com/10.3892/or.2012.1668**.

47 M. Chen, H. Zhang, G. Zhang, A. Zhong, Q. Ma, J. Kai, et al., Targeting TPX2 suppresses proliferation and promotes apoptosis *via* repression of the PI3k/AKT/P21 signaling pathway and activation of p53 pathway in breast cancer, *Biochem. Biophys. Res. Commun.*, 2018, **507**(1), 74–82.

48 C. W. Hsu, Y. C. Chen, H. H. Su, G. J. Huang, C. W. Shu, T. T. L. Wu, et al., Targeting TPX2 suppresses the tumorigenesis of hepatocellular carcinoma cells resulting in arrested mitotic phase progression and increased genomic instability, *J. Cancer*, 2017, **8**(8), 1378–1394.

49 D. R. Matson, R. A. Denu, L. M. Zasadil, M. E. Burkard, B. A. Weaver, C. Flynn, et al., High nuclear TPX2 expression correlates with TP53 mutation and poor clinical

behavior in a large breast cancer cohort, but is not an independent predictor of chromosomal instability, *BMC Cancer*, 2021, **21**(1), 186.

50 D. H. Huang, J. Jian, S. Li, Y. Zhang and L. Z. Liu, TPX2 silencing exerts anti-tumor effects on hepatocellular carcinoma by regulating the PI3K/AKT signaling pathway, *Int. J. Mol. Med.*, 2019, **44**(6), 2113–2122.

51 H. Zarrinnahad, S. A. Dehdast, G. C. Fard, M. Nourbakhsh, M. K. Koohi, G. Panahi, et al., The effect of biosynthesized zinc oxide nanoparticles on gene expression and apoptosis in triple-negative breast cancer cells, *DARU J. Pharm. Sci.*, 2024, **33**(1), 10.

52 S. Sharif, M. S. Lodhi, I. Nayila, A. Irshad, M. Abbas, A. Alotaibi, et al., Phyto-fabrication and characterization of gold nanoparticles by using timur (*Zanthoxylum armatum* DC) and their effect on wound healing, *Open Chem.*, 2024, **22**(1), 20240047, Available from: **https://www.degruyter.com/document/doi/10.1515/chem-2024-0047/html**.

53 M. K. N. Chidambara, G. K. Jayaprakasha, S. M. Mantur and B. S. Patil, Citrus monoterpenes: potential source of phytochemicals for cancer prevention, in *ACS Symposium Series*, ed. B. S. Patil, G. K. Jayaprakasha, K. N. C. Murthy and N. P. Seeram, American Chemical Society, Washington, DC, 2012, pp. 545–558, Available from: **https://pubs.acs.org/doi/abs/10.1021/bk-2012-1093.ch031**.

54 I. Nayila, S. Sharif, M. Shahzad Lodhi, R. Ullah, A. Alotaibi, T. Maqbool, et al., Formulation, characterization and evaluation of anti-breast cancer activity of 2-carene nanoemulsion; *in silico*, *in vitro* and *in vivo* study, *Arab. J. Chem.*, 2024, **17**(9), 105937.

55 S. Kamran, A. Sinniah, M. A. M. Abdulghani and M. A. Alshawsh, Therapeutic potential of certain terpenoids as anticancer agents: a scoping review, *Cancers*, 2022, **14**(5), 1100.

56 L. Zhang, X. Wang, L. Zhang, C. Virgous and H. Si, Combination of curcumin and luteolin synergistically inhibits TNF-α-induced vascular inflammation in human vascular cells and mice, *J. Nutr. Biochem.*, 2019, **73**, 108222.

57 N. M. D. Sandhiutami, W. Arozal, M. Louisa, D. Rahmat and P. E. Wuyung, Curcumin nanoparticle enhances the anticancer effect of cisplatin by inhibiting PI3K/AKT and JAK/STAT3 pathway in rat ovarian carcinoma induced by DMBA, *Front. Pharmacol*, 2021, **11**, 603235, Available from: **https://www.frontiersin.org/journals/pharmacology/articles/10.3389/fphar.2020.603235/full**.

58 M. A. Adahoun, M. A. H. Al-Akhras, M. S. Jaafar and M. Bououdina, Enhanced anti-cancer and antimicrobial activities of curcumin nanoparticles, *Artif. Cells Nanomed. Biotechnol.*, 2017, **45**(1), 98–107.